

Optimization and control of bright, ultrafast laser driven X-ray sources

L. A. Gizzi^{a,#}, A. Giulietti^{a,#}, D. Giulietti^{a,#}, P. Koester^{a,#}, L. Labate^a, T. Levato^{a,#},
F. Zamponi^b, T. Kämpfer^b, I. Uschmann^b, E. Förster^b, R. Sauerbrey^b

^aIPCF-CNR, Area della Ricerca, Via Moruzzi, 1 56124 Pisa, Italy

^bIOQ Institut für Optik und Quantenelektronik, Max-Wien-Platz, 1 07743 Jena Germany

#Also at INFN, Sezione di Pisa, L.go B. Pontecorvo, 3, Pisa, Italy.

ABSTRACT

In this paper we describe recent studies on X-ray emission from ultra-fast laser interactions with solids. We describe the dedicated equipment including a powerful femtosecond, Titanium-Sapphire laser system and custom developed diagnostics for the characterization of both the laser performance and the X-ray emission. We show the experimental results obtained from irradiation of Aluminium and Titanium targets including X-ray yield and spectra obtained using single-photon counting and spectroscopy. We discuss correlation of X-ray emission with the measured properties of hot electrons emerging from the target rear side. In particular, forward accelerated fast electrons propagating through a Ti foil are found to be emitted in a cone perpendicular to the target. A comparison of the experimental findings with the results of a PIC simulation is also reported, aimed at identifying the physical processes responsible for the production of this forward propagating population of fast electrons. Finally, we show results of simple optical spectroscopy measurements of scattered light and we discuss the use of these results in view of optimization and control of this kind of X-ray sources.

Keywords: laser-plasma interactions, X-ray emission, ultrafast

1. INTRODUCTION

Laser-plasmas are well-known for their X-ray emission properties and X-ray sources based on such plasmas are routinely used for a wide range of applications in which high peak power and moderate average power X-ray sources are required [1]. More recently, the development of high repetition rate, powerful femtosecond laser systems is enabling the development of a new generation of laser-driven X-ray sources characterised by a very short pulse duration, well below the pulse duration of synchrotron radiation pulses and comparable with the pulse duration of future fourth generation, LINAC based, X-ray Free Electron Lasers (XFEL).

These sources are based upon the interaction of focused, intense, femtosecond CPA (Chirped Pulse Amplification) [2] laser pulses with a solid targets. This interaction produces *fast* electrons having energies of the order of some tens to a few hundreds of keV [3, 4, 5] that penetrate in the cold target substrate and generate incoherent X-ray fluorescence emission due to K-shell transitions [6]. In principle, X-ray pulses with a duration comparable to the laser pulse duration can be achieved [7] with a relatively small source size [8]. Currently, sources based on this effect provide a unique approach [9] to fs, X-ray probing of matter for the understanding of ultrafast phenomena [10] such as the recently demonstrated non-thermal melting of semiconductors [11].

From the point of view of optimization and control of the properties of these sources, a critical role is played by the mechanisms responsible for the production of the primary *fast* electrons (see for example [12] and [13]). In fact, the main characteristics of $K\alpha$ based ultra short X-ray sources, such as photon yields as well as duration and size, strongly depend upon the production and transport processes of the fast electrons in matter. Therefore the understanding of this issue plays a crucial role when laser-plasma based $K\alpha$ sources have to be modeled and their applications have to be considered (see [14] and references therein).

In particular, for the parameters typical of many smaller-scale laboratory sources of this kind, the resonance absorption and the vacuum heating are expected to be the dominant conversion processes of laser energy into hot electron kinetic energy [15, 16, 17]. In fact, in the case of *p*-polarized laser radiation, efficient energy transfer [18] of

laser energy to the plasma can occur through resonance absorption [19], giving rise to longitudinal electrostatic electron plasma waves (epw) [20]. The subsequent damping of the plasma wave, occurring through collisionless processes, leads to the generation of energetic electrons that can penetrate into the underlying cold target material, where they knock out electrons preferentially from the inner electronic shells of the atoms or ions [21, 22]. In the presence of very steep density gradients, the resonance absorption process is less effective and the vacuum heating [23] can be responsible for the generation of hot electrons [24].

At higher laser intensities, a much more complex scenario sets up which is strongly affected by the presence of precursor radiation [25]. In these circumstances additional mechanisms can take place which account for the actual acceleration of electrons at very high energies. In these circumstances, $K\alpha$ emission spectroscopy of neutral or partially ionized atoms, possibly with spatial resolution, can be exploited for studying the fast electron transport through matter with micrometer resolution [26, 27]. These studies can be relevant to the Fast Ignitor approach to Inertial Confinement Fusion [28,29]. In fact, a major effort has been devoted in the last years to the study, both theoretical and experimental, of important physical issues, such as the return current and the influence of the self-generated electromagnetic fields on the electron transport [30, 31, 32, 15]. From the point of view of applications, this effort yielded important advances like the generation of monoenergetic fast electrons produced in ultrashort laser interactions with solids, as demonstrated by recent dedicated electron diffraction experiments [33,34].

In this paper we report on recent experiments dedicated to the measurement of X-ray yield and the investigation aimed at the identification of the basic mechanisms for the generation of primary electrons. We give an in depth description of the experimental set up used in our experiments along with a detailed account of the observed properties of X-ray fluorescence emission. We report on the measurements of fast electrons on the rear side of the target and a comparison of observations with the predictions of simulations carried out with a Particle-in-cell (PIC) code.

2. THE FEMTOSECOND LASER SOURCE

The main experiments were carried out using the new Ti:Sa system delivering <65 fs pulses with peak power exceeding 2 TW, at the repetition rate of 10 Hz. A schematic view of the entire system is shown in Figure 1. A picture of the actual system is given in Figure 2.

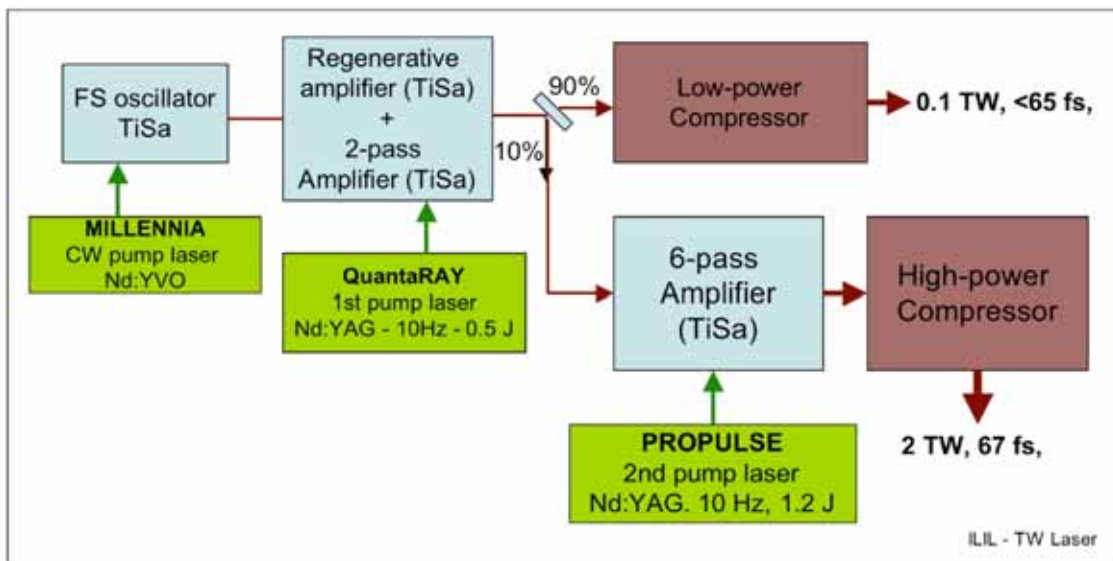


Figure 1. Schematic diagram of the high-power, TW femtosecond laser system at ILIL.

A femtosecond oscillator, a Tsunami (Spectra Physics), pumped by a diode-pumped 5W Nd:YVO, generates sub 50 fs pulses that are stretched and seeded into a regenerative amplifier. The regen. amplifier is pumped by a fraction of frequency doubled, Nd:YAG, Q-switched laser pulses at a 10 Hz repetition rate. After amplification at the 2 mJ level, the stretched pulses are further amplified by a two-pass amplifier pumped by the remaining fraction of the Nd:YAG pulses. The stretched, amplified pulse is then divided in two pulses using a 10%-90% splitter. The pulse containing the larger fraction is compressed and produced a final output of 12 mJ. The remaining pulse is further amplified using a 6-pass

TiSa amplifier pumped by another frequency-doubled Nd:YAG to give a final output of 200 mJ in 65 fs. The temporal and spatial properties of the femtosecond pulses have been characterised in detail using commercial as well as custom developed devices. The temporal profile of the pulse was measured with a custom-made second order auto-correlator based upon non-linear coupling in a 100 μm thick BBO crystal of two focused, equally intense pulses obtained from beam splitting of the full power beam suitably attenuated after a number of reflections by high quality optical flats. The two beams are set to impinge on the crystal with an angle of incidence of approximately 3 deg. The auto-correlation second harmonic (SH) radiation is then emitted along the normal to the target while self-generated SH is collinear with the incident pulses. In our configuration, SH auto-correlation signal is detected in the forward direction while self-generated SH emission of each pulse can be discarded by a simple angular selection.

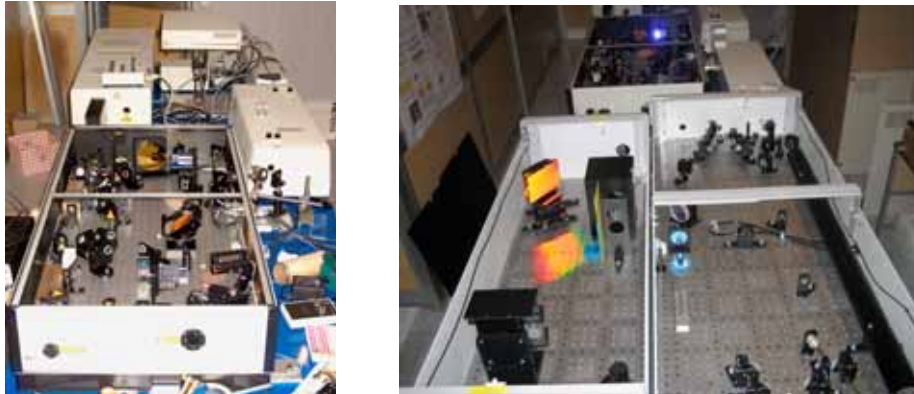


Figure 2. The TiSa laser system at ILIL. Left: mJ front-end system including the oscillator, the Nd:YAG pump laser (top-left) and the regenerative amplifier Right: 6-pass power amplified and pulse compressor.

The autocorrelation curve obtained from a scan of the delay of approximately 1 ps around the maximum SH signal is shown in Figure 3 (left). The data points fitted with a double Gaussian function, to take into account the low intensity tails of the curve, yield a FWHM of 67 fs. The curve on the Figure 3 (right) shows the high dynamic range autocorrelation curve over a temporal range of 200 ps before the main pulse. According to this plot, the contrast of our system due to amplified spontaneous emission (ASE) is better than 10^8 . A number of replica pulses are also present before the pulse whose contrast is better than 10^5 .

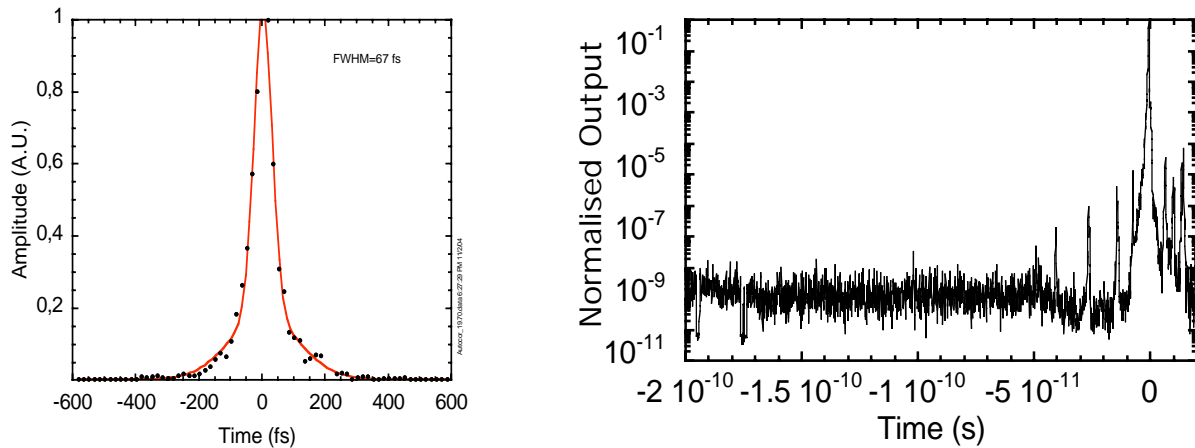


Figure 3. (Left) Autocorrelation curve of the full power pulse. (Right) High dynamic range autocorrelation trace (Amplitude Tech. Sequoia) of the laser pulse after the regenerative amplifier.

The spatial quality of the laser pulse was also studied by means of an equivalent plane monitor (EPM) based on a 100 cm nominal focal length optics and a 12 bits CCD camera (a Photometrics *Sensys*) with a pixel size of 8 μm edge. Figure 4 shows an image of the beam taken with the EPM at a distance of 7.5 cm before the best focus of the 100 cm optics. The plot on the right shows a lineout of the beam image fitted with a Gaussian curve.

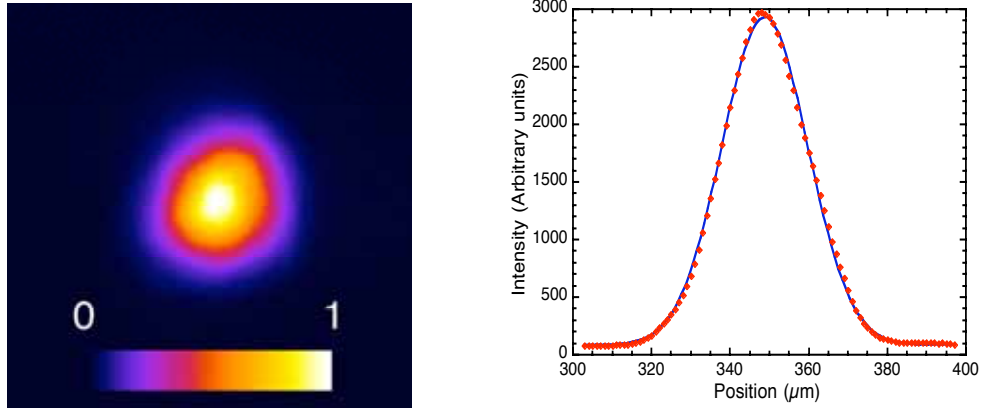


Figure 4. (left) Equivalent plane imaging of the laser beam taken at a distance of 7.5 cm before the nominal focal position of a 100 cm focal length. (right) Horizontal lineout (taken along the diameter) of the beam image on the left. The solid line (blue in the color version), shows the best fit obtained with a Gaussian function.

Both the temporal and spatial data show a high quality femtosecond pulse, focusable in a spot size very close to the diffraction limit. Scaling the focal spot size (FWHM) obtained by a 100cm focal length equivalent plane monitoring to the 10 cm focal length typically used in our experiments, we can assume a FWHM focal spot of approx. 11 μm . Considering the pulselength of 67 fs and an energy of 12 mJ we find that the peak intensity on the target can exceed 10^{17} W/cm^2 . In the case of the 200mJ the pulse is focused on target using a gold coated, off-axis parabolic mirror to reach peak intensities of $5 \times 10^{18} \text{ W/cm}^2$.

3. EXPERIMENTAL SET UP

A range of diagnostic arrangements were adopted for the detection and measurement of primary parameters of X-ray bursts produced in the experiment, as shown in the experimental set-up drawn schematically in Figure 5. In the typical configuration, the laser pulse is focused using an $f/20$ lens onto the surface of a flat (solid or foil) target at an angle of incidence of about 40° . The target foil is moved horizontally or vertically to ensure a fresh interaction surface for each laser pulse in the series of multi-shot measurements. The size of the focal spot was evaluated by means of an equivalent plane monitor technique to be of about 15 μm . The Rayleigh length is approximately 400 μm . Considering these values, the peak intensity on the target can be estimated to be $I_L = 5 \times 10^{16} \text{ W/cm}^2$. We observe here that the relatively long Rayleigh length ensures that a plane wave is interacting with the target, even for small displacements from the focal spot, so that a well defined laser wavevector exists whose direction can be safely identified with respect to that of the detected electrons.

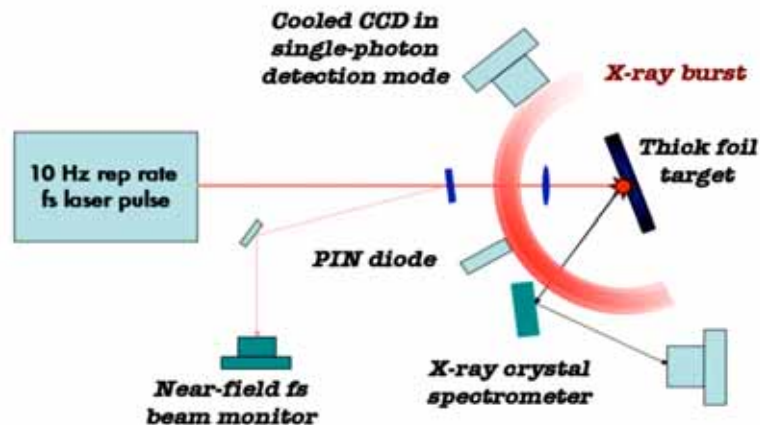


Figure 5. Schematic view of the experimental set up for the generation and detection of short pulse X-ray radiation from intense laser-solid interaction. The gradient-filled circular sector represents schematically the burst of X-rays originating from the target and emerging only from the front side of the target, emission from the rear-side being absorbed as in the case of very thick target substrate.

The fast electrons generated during the interaction and passing through the Ti foil were detected by means of a stack of dose-sensitive radiochromic films placed behind the target, at a distance of about 5 mm from it. The energy and the angular distribution of the electrons could be retrieved by means of an original reconstruction algorithm [35] based upon a Montecarlo simulation employing the CERN library GEANT 4.2.0 [36]. We observe here that energetic particles leaving a detectable signal onto the radiochromic films were identified as electrons since the usage of proton sensitive CR39 films led to a null result.

High resolution spectroscopy of X-ray emission was performed using two types of detectors. One was based upon flat or bent crystals arranged in a first order Bragg configuration [37, 38, 39] for the high resolution characterization of spectral properties. X-ray emission was also analyzed using a back-illuminated cooled CCD detector (Princeton Instruments) placed at about 1 meter from the source. This distance allowed the CCD detector to operate in single photon regime [17]. As it is well-known, provided the detector response to different energy photons is known, this detection technique enables the spectral properties as well as the incident X-ray flux to be simultaneously measured [40]. In fact, it is now well established that each event detected by the CCD can be analysed to retrieve the actual charge produced in the CCD pixels. This charge can then be converted into the incident X-ray photon, via independent energy calibration [40]. We made extensive use of this technique to measure properties of X-ray emission and an account of the main results in this field is given below.

4. THE TI-K α SOURCE

This X-ray detection technique was preliminarily used to investigate the effect of a change of focused intensity due to change of CPA pulse duration in the sub-ps level. In this case, the change of pulse duration was achieved by changing the configuration of the final compressor of the TiSa laser system. The plot of Figure 6 (left) shows the single-event spectra obtained with 250 fs (black line) and 500 fs pulses (blue line) containing the same energy of approx. 12 mJ. Both spectra show a line emission the K α Al line at 1486 eV partially merged with a low intensity He-alpha from He-like Al plasma at 1598 eV as shown in detail in the plot of Figure 6 (center). Both spectra show a rapidly decreasing high energy component. In the higher laser intensity case, this component extends up to 30 keV range with an additional peak just below 40 keV.

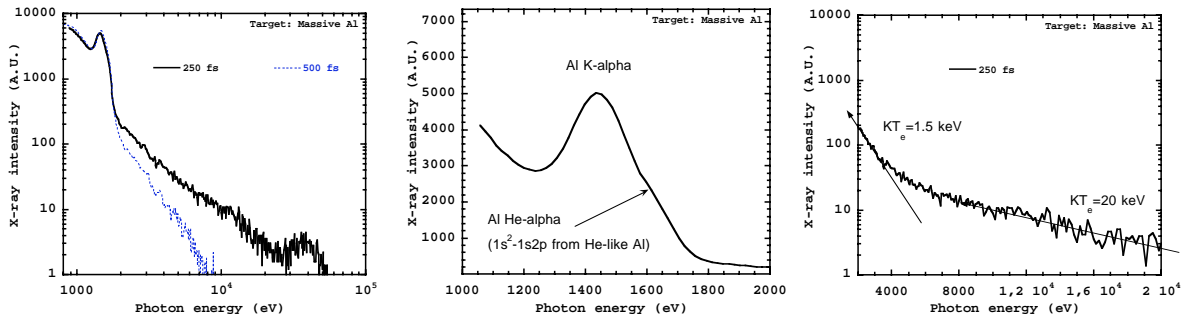


Figure 6. (left) Single photon spectra obtained from laser irradiation of a solid Al target irradiated by a 10 mJ laser pulse at two different values of the pulse duration, namely 250 fs (black line) and 500 fs (blue line). (right) (center) Expanded plot of the line-emission component of the spectrum showing the main K α line and the contribution of line emission from He-like Al plasma. (right) Exponential fit of the higher energy portion of the 250 fs curve.

The rapidly decreasing part of the spectrum is shown in detail in Figure 6 (right). Also shown in the figure is the exponential fit for the lower and higher energy end of the plot. According to this fit, the higher energy end of the X-ray spectrum decreases exponentially with a coefficient of 20 keV. Assuming that this parameter is linked to the energy distribution function of fast electrons, according to the model of fast electron generation [41], the electron energy is related to the $I\lambda^2$ parameter of the incident laser light according to the following relation:

$$T_{hot} = \left[\sqrt{1 + \frac{I\lambda^2}{2.8 \times 10^{18}}} - 1 \right] 511 \text{ (keV)}.$$

At the incident laser intensity of approximately $5 \times 10^{16} \text{ W/cm}^2$ (expected for the partially compressed pulse of 250 fs) corresponding to the data plotted in Figure 6 (right), the fast electron temperature is expected to be in the 10 keV range,

a value consistent with the observed one. A more detailed modelling of fast electrons requires dedicated numerical simulations and will be discussed below.

The plot of Figure 7 shows $K\alpha$ emission from a 12.5 μm thick Ti target, irradiated with a 12 mJ pulses with a pulse length optimised at 67 fs (FWHM) for an intensity on target of $2 \times 10^{17} \text{ W/cm}^2$. The main emission component due to the $K\alpha$ line at 4.51 keV is clearly visible in the plot. Also visible in the plot is the so-called escape peak, due to energy loss of one Si $K\alpha$ photon arising from interaction of primary photoelectrons generated by the incident Ti- $K\alpha$ photons in the CCD pixels.

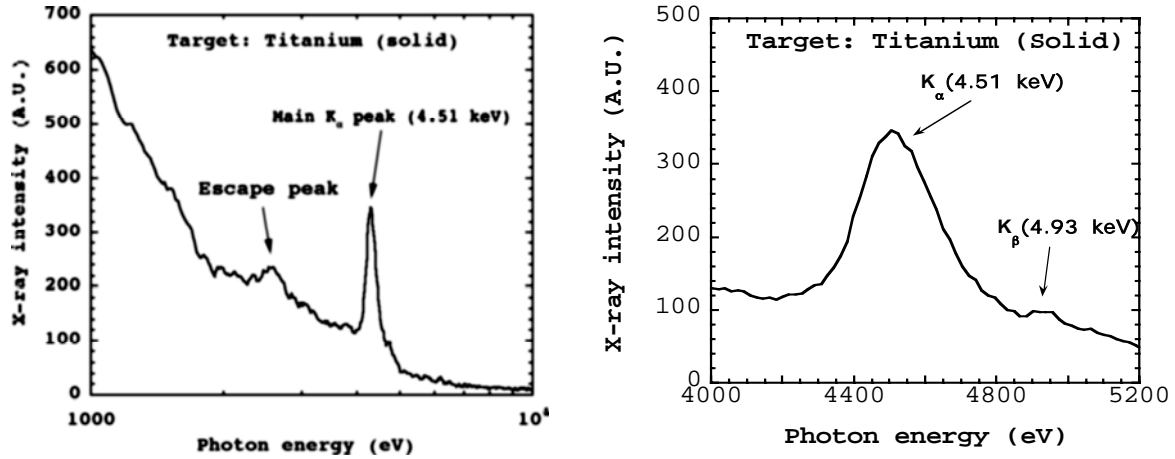


Figure 7. Spectrum of the X-ray emission produced during the irradiation of a solid Ti target by a 67 fs laser pulse at an intensity above 10^{16} W/cm^2 . The main line visible in the spectrum is the Ti $K\alpha$ line at 4.51 keV. Also visible on the low energy side of the Ti $K\alpha$ line is the so-called escape peak due to loss of Si $K\alpha$ photons in the CCD silicon active layer. The plot on the right shows that the $K\beta$ line at 4.93 keV is also visible.

The detection technique used to obtain the spectra of Figure 7 enabled us to obtain simultaneously the total flux of X-ray photons emitted by the source at the Ti- $K\alpha$ photon energy. In fact, as discussed above, the CCD based technique used in our experiments enabled us to measure the photons emitted by the source at every laser shot. Taking into account the solid angle of view of the CCD and assuming an isotropic distribution of emission, we find out that our X-ray source emits approximately 10^7 photons per pulse at 4.51 keV. Since the source can operate at a repetition rate of 10 Hz, that is the rep-rate of the driving laser pulse, we estimate an average X-ray power of 70 nW. A summary of the main parameters of our source-operating regime is given in Table 1.

TARGET	PHOTON ENERGY	TOTAL FLUX	REP-RATE	DIVERGENCE	PULSE DURATION	SOURCE SIZE
Ti	4.51 keV	10^7 per pulse	10 Hz	Isotropic	$\ll 1 \text{ ps}$	$\approx 10 \mu\text{m}$

Table 1. Summary of main parameters of the laser-driven, ultra-fast X-ray source running with the Ti target.

We point out here that the main attractiveness of this class of sources is the short duration of the X-ray pulses. In general, the X-ray pulse duration will be mainly determined by the driving laser pulse duration. However, several interaction parameters including the target geometry, will contribute to lengthening the pulse. Although a direct measurement of our X-ray pulse duration has not been carried out yet, measurements performed in similar experimental conditions [42] show that in the case of 100 fs laser pulse, an X-ray pulse-length between 200 fs and 600 fs may be expected. It is reasonable to assume that in our set up, a similar X-ray pulse will be achieved.

5. MEASUREMENTS AND MODELING OF FAST ELECTRONS

In this paragraph we show the result of experimental measurements dedicated to the analysis of fast electrons generated during the laser-target interaction and emitted forward through the target. These measurements are aimed at providing information on the electron distribution function of primary electrons that give rise to the X-ray emission.

A set of 2 layers of radiochromic films (HD810 radiochromic layers enclosed in an Al-foil pack) were used to detect energetic electrons generated in the interaction experiment. Figure 8 shows the grayscale readout of the first RC film layer after exposure to electrons emitted during a sequence of 100 *p*-polarized laser shots on a 12.5 μm Ti target.

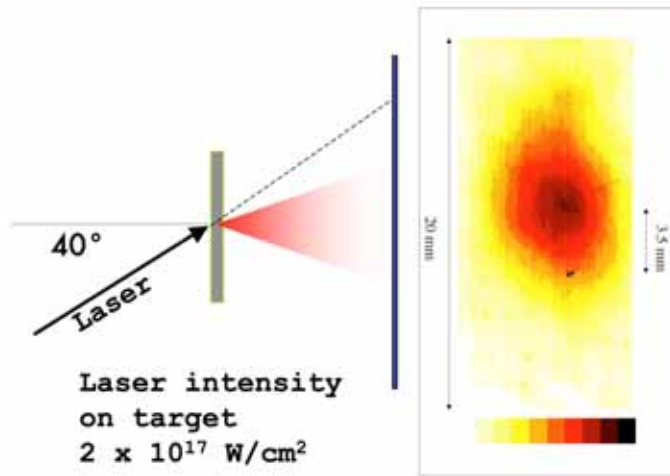


Figure 8. Image of the RC film exposed to fast electrons emitted in the forward direction by the laser-target interaction. The result was obtained from a sequence of 100 *p*-polarized laser shots.

A broad spot is clearly visible in the lower part of the RC film image as a result of the release of dose in the sensitive layer of the RC film. According to the geometry of the experiment, this spot corresponds to electrons propagating in the direction of the target normal and passing through the target. A marker (not visible in the figure) of the laser beam direction on the film, obtained by direct laser heating, enabled us to define a reference for the direction of the laser beam. The properties of the electrons forming the broader spot can be estimated by means of Monte Carlo simulations accounting for the energy deposition in each of the RC film layers as stacked in our experimental conditions. Figure 4 shows the energy released by an electron in the first two layers of the stack as a function of its kinetic energy when leaving the rear side of the target. According to the plot and taking into account the detection threshold of the RC films, since no detectable signal was typically observed in the second layer, an energy of some tens up to a few hundreds of keV can be estimated for the electrons emitted forward, perpendicularly to the target surface, which are responsible for the signal visible in figure 3.

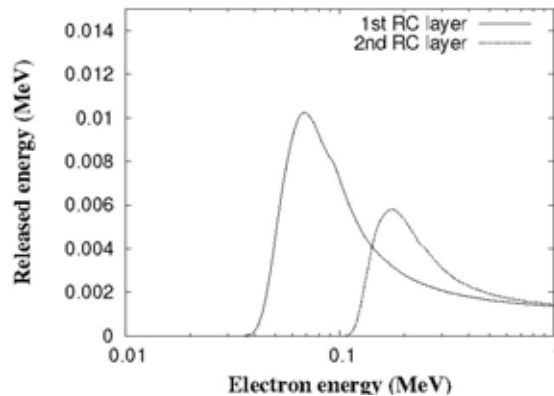


Figure 9. Energy released by an electron in each of the first two RC films in our experimental conditions as a function of the electron kinetic energy. Calculations are shown based on the Monte Carlo library GEANT 4.2.0 [].

As discussed above, the production of a population of hot electrons is very important in the interaction of ultrashort laser pulses with solids and in the optimization of X-ray $K\alpha$ sources. Depending on the fundamental mechanism(s) leading to the production of these electrons, different scaling laws have been proposed for the electron temperature as a function of the laser intensity, either on the basis of PIC simulations or based upon experimental data.

As already done above in the case of partially compressed pulses (250 fs), it is interesting to compare the hot electron temperature obtained from our experiments with the one expected by more detailed and recent models proposed in literature. In fact, the scaling law suggested by PIC codes [43] becomes $T_{hot} \approx 110 (I_{17})^{1/2}$ keV, where I_{17} is the laser intensity in units of 10^{17} W/cm². In our case, this would give an electron temperature of about 77 keV. As we will see below, this value is in a good agreement with the prediction of our PIC simulations where the temperature of the electrons having their momentum in a well-defined cone with respect to the target normal was investigated. A different scaling law has been suggested in [22], based upon experimental data. In our case, this law would give a lower electron temperature compared to the observed one.

Beside their temperature, the distribution of the initial propagation direction of the fast electrons is of a major concern when the size of the X-ray emission region has to be considered in ultrashort laser-plasma K α sources. This is, actually, a quite complex task, as it depends upon a number of parameters (see for example [44] and references therein).

In our experiment, an estimate of the angular spread of the electrons passing through the target can be retrieved, neglecting the space-charge effect of the electron bunch, by considering the size of the spot produced onto the RC film. By simple geometrical considerations, the result displayed in Figure 8 accounts for an aperture angle of 17° HWHM for the angular spread of the observed electrons.

In order to gain some insights on the physical processes leading to the production of hot electrons emitted forward perpendicularly to the target surface in our experiment, 2D simulations were carried out by means of a PIC (Particles-In-Cell) code. In our simulations the femtosecond laser pulse impinges on a target after a low level prepulse due to ASE. The initial density map was set according to the results of hydrodynamics simulations performed using the code POLLUX [45]. To this purpose, the pre-plasma was considered to be produced by a gaussian pedestal of the main pulse with duration $\tau_{ASE} = 7$ ns and intensity $I_{ASE} = 5 \times 10^{10}$ W/cm². According to these simulations, a pre-plasma with a density scalelength at the critical density $L_{n@nc} < \lambda_L$, λ_L being the laser wavelength, can be expected in our experimental conditions. The PIC simulations show that most of the fast electrons are generated in a thin layer around the critical surface. The plot of Figure 10 shows the energy distribution predicted by the code for the electrons having the direction of their momentum in a cone of semi-aperture 17° with respect to the inward normal to the target surface. A double Maxwellian function fit to the data is also shown in the figure.

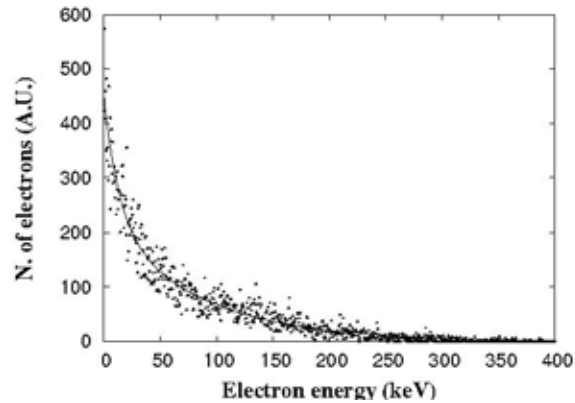


Figure 10. Energy distribution of the electrons having their momentum oriented in a cone of semiaperture 17° with respect to the inward normal to the target surface, as retrieved by a PIC simulation. The curve resulting from a fit with a 2 Maxwellian function is also shown.

According to this fit, the main temperature expected for forward propagating electrons is approximately 83 keV, a value in a good agreement with theoretical and numerical models given in the literature (see for example [46,47,24]). These considerations suggest that a major role is played in our experimental conditions by the resonance absorption or the vacuum heating processes. This is confirmed by the measurement of the K α emission yield as a function of the laser polarization. Such a study has been carried out in our case by inserting a rotating half-wave plate in the beam path before the focusing lens. The laser system is *p*-polarized at the exit of the laser system. By rotating the half-wave plate, the polarization of the laser radiation can be changed continuously from *p* to *s*. In our experiment, the polarization was changed stepwise from *p* to *s* and again to *p*. For each polarization direction, the signal from the CCD detector was considered as a measure of the K α emission yield. Figure 11 shows this quantity as a function of the rotation angle of the half-wave plate. A strong dependence of the X-ray yield on the polarization of the laser light is clearly visible, being more than one order of magnitude higher for *p*-polarized laser light than for *s*-polarized one.

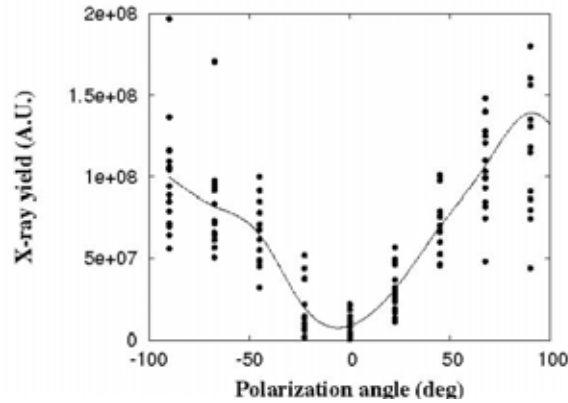


Figure 11. X-ray emission yield as a function of the polarization angle of the laser beam. The angle $\vartheta = 0^\circ$ corresponds to an *s*-polarized beam and the angles $\vartheta = \pm 90^\circ$ correspond to a *p* polarized beam.

Although we are not able here to clearly identify which one of the resonance absorption or vacuum heating processes is predominating since we are in an experimental regime in which both of them can be expected, this result indicates that interaction at the critical density layer is playing the dominant role in our interaction.

6. TOWARDS MULTI-WAVELENGTH X-RAY $K\alpha$ SOURCES

As shown above, fast electron generation and transport plays a key role in the modelling of $K\alpha$ generation in the femtosecond regime. As already discussed above, electron transport issues are of a great relevance when higher laser intensities are used to generate higher energy and, possibly, higher current beams of fast electrons. Recently, an experimental campaign was carried out at the Jena laser facility to address fast electron propagation issues. The aim of the experiment was the investigation of dynamics of propagation of energetic electrons produced by ultra-short laser irradiation of solid targets. To this purpose, multi-layer targets were irradiated using the 10TW, Ti:Sa laser pulses at an intensity exceeding 10^{19} W/cm². Front and rear side X-ray imaging was used to detect propagation of electrons through the cold multi-layer target substrate. As shown in the schematic set-up of Figure 12, optical spectroscopy was set up to monitor the generation of integer (2ω) and half-integer ($3\omega/2$) harmonics of the fundamental, 800 nm radiation. In the same experiment, direct angular and spectral measurement of the energetic electrons emitted in the forward direction was also carried out. $K\alpha$, monochromatic imaging of the X-ray source was accomplished by using two pin-hole cameras equipped with 5 μ m pin-holes and a full depletion, back-illuminated, cooled charge coupled devices (CCD). The cameras were set to operate in the single-photon regime to enable selection of $K\alpha$ photons. This technique enabled simultaneous spectral and spatial imaging of the X-ray photons to achieve monochromatic images at the $K\alpha$ energy typical of each layer.

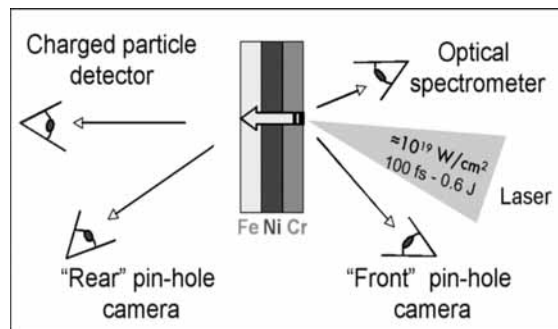


Figure 12. Schematic experimental set-up for the study of fast electron propagation in multi-layered targets. Each target layer was 10 μ m thick. Pin-hole cameras were equipped with cooled CCD cameras and were arranged to work in a near-single-photon regime to enable photon energy selection.

Here we focus our attention on the overall spectral features of the radiation emitted by our target. The plots of Figure 13 show the total spectrum obtained by adding up spectra of a set of seven hundred pin-hole camera images.

Clearly visible is the $K\alpha$ emission from Cr and Ni layers in the front detector (dotted line) and Cr, Fe and Ni in the rear detector (solid line). Fe emission, just visible in the front detector, is strongly attenuated by absorption in the Cr substrate

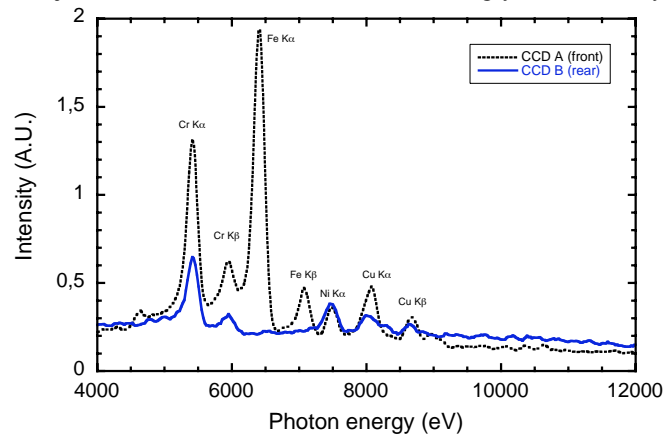


Figure 13. X-ray spectrum of front and rear emission from irradiation of a Cr-Ni-Fe, multi-layer target irradiated by a femtosecond laser pulse at an intensity of 10^{19} W/cm².

According to these results, the use of multi-layer targets can be successful in generating multi-wavelength X-ray radiation characteristic of each layer of the target. These circumstances indicate that the fast electron beam generated during the interaction propagates efficiently through the different layers. A detailed analysis of the dynamics of propagation of fast electrons is beyond the aim of the present work. However, it is interesting to observe that, according to preliminary analysis of the monochromatic images taken at the different $K\alpha$ energies for each layer, limited source broadening is found to occur through the layers. This observation suggests that the component of the electron beam from which $K\alpha$ originates propagates without a significant divergence. This conclusion certainly applies to the low-energy tail (up to ≈ 50 keV) of the fast electron population that has the higher probability of producing $K\alpha$ radiation. The same may be true at higher energy (1 MeV and above) electron energy, where the Ti ionization cross sections increases again. Measurements were also carried out on the electrons leaving the target in the forward direction, as already done in the experiment described in the previous section. The angular distribution of the high energy (>0.3 MeV) electrons indicates a significant divergence, similar to the one Figure 8. In this case, however, a much higher energy, up to 1 MeV was found, and a detailed investigation of the correlation between angle of emission and energy of electrons is still in progress. In fact, it should be noted here that these results were obtained at much higher laser intensity than in the case discussed in the previous section. Therefore, a direct comparison of the two results is not straightforward. Indeed, at higher laser intensity, additional mechanisms can take place which can account for the production and the acceleration of fast electrons.

7. OPTICAL SPECTROSCOPY

The above considerations should also be carefully taken into account when trying to optimize interaction conditions for X-ray emission in terms of efficiency and source size. In fact, at higher intensities, beside the above cited mechanisms, additional non-linear mechanisms may account for energy transfer from the laser pulse to energetic electrons which may influence X-ray conversion efficiency. Two-plasmon decay and Raman scattering are examples of mechanisms that are well known for their influence on the electron distribution function [48]. In fact, energy transferred to electron-plasma waves at approximately half of the fundamental laser frequency, is ultimately converted into energetic electrons via collisionless damping of such waves. A clear signature of the occurrence of these processes is the generation of half-integer harmonics of the fundamental laser frequency [49] resulting from the non-linear coupling of electron plasma waves and fundamental laser radiation and/or its integer harmonics. This emission can be easily detected and monitored using standard optical spectroscopy. Optical spectroscopy can also be used to investigate directly second harmonic emission whose generation, depending on the direction of propagation, can be attributed to wave coupling at the critical density [17] or to sum-frequency of incident and back-scattered laser light [50].

In the same experiment described in the previous paragraph, optical spectroscopy of fundamental, second and three-half harmonic scattered specularly by the target was indeed used to monitor reproducibility of interaction conditions from shot to shot. The plot of Figure 14 shows a typical spectrum of light detected in the specular direction with respect to the

incident laser light. The spectrum was obtained at an intensity of 10^{18} W/cm² and clearly shows the 2ω emission at 400nm and a broader $3/2\omega$ emission centred at approximately 550nm.

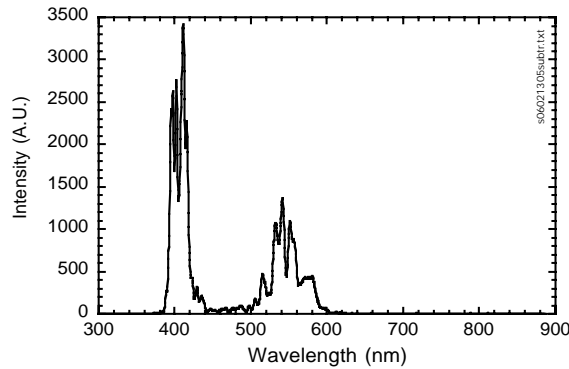


Figure 14. Sample spectrum of specularly reflected light obtained from low-energy (100mJ) laser interaction with a $5\mu\text{m}$ thick Ti foil. A rejecting filter was used to stop the 800nm laser light reflected by the target.

Thanks to the large number of shots required by the experiment, a significant number of spectra could be acquired. The analysis shows that 2ω and $3/2\omega$ exhibit significant changes of intensity from shot to shot. The emission at $3/2\omega$ is characterized by a single, broad peak centered at the nominal $3/2\omega$ value. In some cases, a double-peak structure was also observed. These changes may be due to shot by shot fluctuations of initial interaction parameters like laser energy, laser intensity, target surface imperfections. A correlation of optical data with X-ray emission could also be investigated. Here we show a preliminary result of this investigation showing the sequence of the optical spectra including second harmonic and three-half harmonic components. The plots of Figure 15 show the behavior of optical scattering over 250 shots. Each spectrum acquired in the spectral region (approx. from 350nm to 600nm) including second harmonic (2ω), and three-half harmonic ($3/2\omega$), is displayed as a false color vertical line. Also shown in the same figure is the X-ray emission detected simultaneously by a pin-hole camera equipped with a CCD detector. The sequence was re-sorted with increasing X-ray flux level.

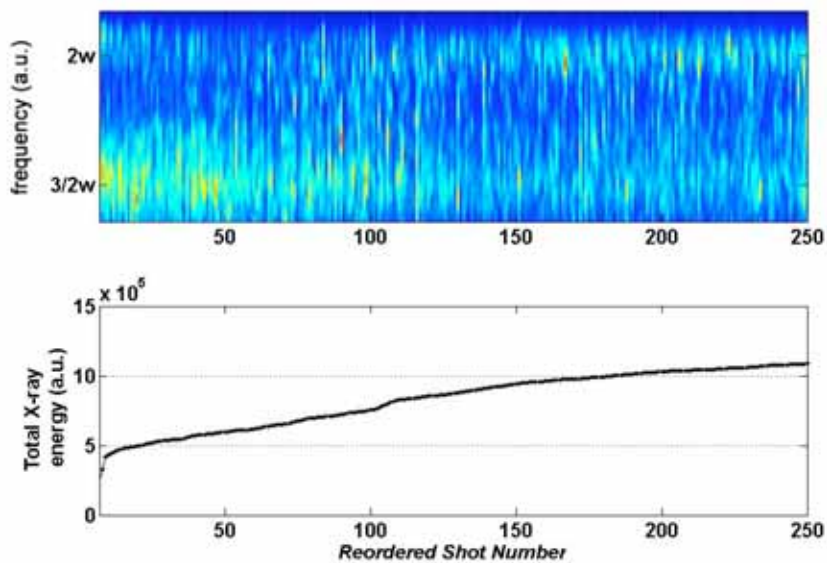


Figure 15. Sequence of optical spectra (top) of light scattered in the specular direction in the interaction of a 90 fs laser pulse with a thick foil target. The intensity on target was greater than 10^{19} W/cm² and the angle of incidence was approximately 12 degrees. The plot (bottom) shows the total X-ray flux detected by the CCD in the range up to ≈ 10 keV. The sequence is sorted with increasing X-ray flux level.

Here we are interested in knowing the potential of this simple optical diagnostic as a marker of an efficient X-ray conversion. Considering that the CCD specifications and the X-ray filters used, the accessible X-ray region ranged between 1 keV and 15 keV and included $K\alpha$ emission from the target. The plot of Figure 15 (bottom) shows the behavior of X-ray emission flux.

If we restrict our analysis to the shot index number below 250, this plot immediately shows that X-ray emission intensity is correlated with 2ω emission and is anti-correlated with $3/2\omega$ emission. This is fully consistent with a simple picture in which strong interaction occurs in the pre-plasma where laser-induced instabilities (SRS and TPD) can more effectively grow. At the same time, laser light cannot propagate efficiently up to the critical density layer where resonance absorptions and/or vacuum heating may take place. These circumstances will preferentially lead to the production of very energetic electrons in the electron plasma electron plasma waves. These electrons will easily escape from the target resulting in a less efficient X-ray emission. In contrast, when low $3/2\omega$ emission and higher 2ω emission occur, laser energy is expected to couple more efficiently with the higher density region of the target plasma. These circumstances fall in the scenario discussed above and are certainly of a greater interest for multi keV X-ray source optimization.

8. SUMMARY AND CONCLUSIONS

A description of the experimental work recently carried for the characterization of ultrashort X-ray source based on the $K\alpha$ emission from solid targets has been given. In particular, the issues related to the production of the hot electron population, which is responsible for the X-ray emission, have been studied using diagnostics for both the X-ray emission and the forward accelerated electrons. X-ray emission yield clearly demonstrates that the most effective absorption mechanism is resonance absorption. Electrons having energies up to some hundreds of keV and passing through the Ti foil have been observed both experimentally and numerically. A study of the mechanisms responsible for their production and of their angular distribution is still ongoing, based on hydrodynamic and PIC simulations.

A preliminary result of a spectroscopic investigation on light scattered in the specular direction was presented in which X-ray emission was found to be strongly correlated with 2ω emission and anti-correlated with $3/2\omega$ emission. These measurements suggest a simple way of monitoring interaction conditions occurring in laser-driven femtosecond X-ray sources. In this way, shot by shot reproducibility of the required interactions conditions may be monitored and, possibly, controlled.

ACKNOWLEDGEMENTS

This work was partially supported by the MIUR project 'Impianti innovativi multiscopo per la produzione di radiazione X e ultravioletta' (L. 449/97) and by the INFN PLASMON-X project. We would like to thank A. Barbini, W. Baldeschi and M. Voliani for technical assistance.

REFERENCES

- 1 D. Giulietti and L.A. Gizzi, "X-ray emission from laser-produced plasmas", *La Rivista del Nuovo Cimento* 21, 1 (1998).
- 2 D. Stikland and G. Mourou, "Compression of amplified chirped optical pulses", *Opt. Commun.* 56, 219 (1985).
- 3 Th. Schlegel, S. Bastiani, L. Gremillet, J.-P. Geindre, P. Audebert, J.-C. Gauthier, E. Lefebvre, G. Bonnaud, and J. Deletrez. "Comparison of measured and calculated x-ray and hot-electron production in short-pulse laser-solid interactions at moderate intensities", *Physical Review E*, 60, 2209–2217 (1999).
- 4 K. B. Wharton, S. P. Hatchett, S. C. Wilks, M. H. Key, J. D. Moody, V. Yanovsky, A. Offenberger, B. A. Hammel, M. D. Perry, and C. Joshi. "Experimental measurements of hot electrons generated by ultraintense ($> 10^{19}$ W/cm²) laser-plasma interactions on solid-density targets", *Physical Review Letters*, 81, 822–825 (1998).
- 5 D. Salzmann, Ch. Reich, I. Uschmann, E. Foerster, and P. Gibbon. "Theory of $k\alpha$ generation by femtosecond laser-produced hot electrons in thin foils", *Physical Review E*, 65, 036402, (2002).
- 6 A. Rousse, P. Audebert, J. P. Geindre, F. Fallies, J. C. Gauthier, A. Mysyrowicz, G. Grillon, and A. Antonetti. "Efficient $k\alpha$ x-ray source from femtosecond laser-produced plasmas", *Physical Review E*, 50, 2200–2207 (1994).
- 7 Ch. Reich, I. Uschmann, F. Ewald, S. Duesterer, A. Luebcke, H. Schwoerer, R. Sauerbrey, and E. Foerster, "Spatial characteristics of $k\alpha$ x-ray emission from relativistic femtosecond laser plasmas", *Physical Review E*, 68, 056408 (2003).
- 8 T. Feuer, A. Morak, I. Uschmann, Ch. Ziener, H. Schwoerer, Ch. Reich, P. Gibbon, E. Foerster, and R. Sauerbrey, "Femtosecond silicon $k\alpha$ pulses from laser-produced plasmas", *Physical Review E*, 65, 016412 (2001).
- 9 C. Rose-Petrucci et al., "Picosecond-milliangstrom lattice dynamics measured by ultrafast X-ray diffraction", *Nature*, 398, 310 - 312 (1999).

-
- 10 A. Rousse, C. Rischel, J.-C. Gauthier, “Femtosecond X-ray crystallography”, *Rev. Modern Physics* **73**, 17 (2001).
- 11 A. Rousse et al., “Non-thermal melting in semiconductors measured at femtosecond resolution”, *Nature*, **410**, 65 - 68 (2001).
- 12 S. C. Wilks and W. L. Kruer. “Absorption of ultrashort, ultra-intense laser light by solids and overdense plasmas”. *IEEE Journal of Quantum Electronics*, 33, 1954–1968 (1997)
- 13 G. Malka, M. M. Aleonard, J. F. Chemin, G. Claverie, M. R. Hartson, J. N. Scheurer, V. Tikhonchuk, S. Fritzler, V. Malka, P. Balcou, G. Grillon, S. Moustazis, L. Notebaert, E. Lefebvre, and N. Cochet, “Relativistic electron generation in interactions of a 30 TW laser pulse with a thin foil target”. *Physical Review E*, 66, 066402 (2002).
- 14 J. R. Davies. “How wrong is collisional monte carlo modeling of fast electron transport in high-intensity laser-solid interactions?”, *Physical Review E*, 65, 026407 (2002).
- 15 J. Zhang, Y. T. Li, Z. M. Sheng, Z. Y. Wei, and X. Dong, Q. L. Lu, “Generation and propagation of hot electrons in laser-plasmas”, *Applied Physics B*, 80, 957–971 (2005).
- 16 P. Gibbon and E. Foerster. “Short-pulse laser-plasma interactions”, *Plasma Physics and Controlled Fusion*, 38, 769–793, (1996).
- 17 L. A. Gizzi, A. Giulietti, D. Giulietti, P. Audebert, S. Bastiani, J.-P. Geindre, and A. Mysyrowicz. “Simultaneous measurements of hard x-rays and second-harmonic emission in fs laser-target interactions”. *Physical Review Letters*, 76, 2278–2281, (1996).
- 18 L.A.Gizzi, A.J.Mackinnon, D.Riley, S.M.Viana, O.Willi, “Measurements of thermal transport in plasmas produced by picosecond laser pulses”, *Laser Part. Beams*, **13** (1995) and references therein.
- 19 D. Riley, J. J. Angulo-Gareta, F. J. Khattak, M. J. Lamb, P. S. Foster, E. J. Divall, C. J. Hooker, A. J. Langley, R. J. Clarke, and D. Neely, “K α yields from Ti foils irradiated with ultrashort laser pulses”, *Physical Review E*, 71, 016406 (2005).
- 20 D.Riley, L.A.Gizzi, A.MacKinnon, S.M.Viana, O.Willi, “Absorption of High Contrast 12 ps UV Laser Pulses by solid targets”, *Phys. Rev. E*, **48**, 4855 (1993).
- 21 F. Ewald, H. Schwoerer, and R. Sauerbrey. “K α radiation from relativistic laser-produced plasmas”, *Europhysics Letters*, 60, 710–716, (2002).
- 22 S. B. Hansen, A. Ya. Faenov, T. A. Pikuz, K. B. Fournier, R. Shepherd, H. Chen, K. Widmann, S. C. Wilks, Y. Ping, H. K. Chung, A. Niles, J. R. Hunter, G. Dyer, and T. Ditmire, “Temperature determination using ka spectra from M-shell Ti ions”, *Physical Review E*, 72, 036408 (2005).
- 23 F. Brunel, “Not-so-resonant, resonant absorption”, *Physical Review Letters*, 59, 52–55, (1987).
- 24 P. Gibbon and A. R. Bell “Collisionless absorption in sharp-edged plasmas”, *Physical Review Letters*, 68, 1535–1538, (1992).
- 25 D.Giulietti, L.A.Gizzi, A.Giulietti, A.Macchi, D.Teychenneé, P.Chessa, A.Rousse, G.Cheriaux, J.P.Chambaret, G.Darpenigny, “Observation of solid-density laminar plasma transparency to intense 30-femtosecond laser pulses,” *Phys. Rev. Lett.* **79**, 3194 (1997).
- 26 R. Freeman, C. Anderson, J. M. Hill, J. King, R. Snavely, S. Hatchett, M. Key, J. Koch, A. MacKinnon, R. Stephens, and T. Cowan, “Understanding the role of fast electrons in the heating of dense matter: experimental techniques and recent results”, *Journal of Quantitative Spectroscopy and Radiative Transfer*, 81, 183–190 (2003).
- 27 H. Nishimura, T. Kawamura, R. Matsui, Y. Ochi, S. Okihara, S. Sakabe, F. Koike, T. Johzaki, H. Nagatomo, K. Mima, I. Uschmann, and E. Foerster, “K α spectroscopy to study energy transport in ultrahigh-intensity laser produced plasmas”, *Journal of Quantitative Spectroscopy and Radiative Transfer*, 81, 327–337 (2003).
- 28 A. Macchi, A. Antonicci, S. Atzeni, D. Batani, F. Califano, F. Cornolti, J. J. Honrubia, T. V. Lisseikina, F. Pegoraro, and M. Temporal, “Fundamental issues in fast ignition physics: from relativistic electron generation to proton driven ignition”, *Nuclear Fusion*, 43, 362–368, (2003).
- 29 M. H. Key, M. D. Cable, T. E. Cowan, K. G. Estabrook, B. A. Hammel, S. P. Hatchett, E. A. Henry, D. E. Hinkel, J. D. Kilkenny, J. A. Koch, W. L. Kruer, B. Langdon, A. B. F. Lasinski, R. W. Lee, B. J. MacGowan, A. MacKinnon, J. D. Moody, M. J. Moran, A. A. Offenberger, D. M. Pennington, M. D. Perry, T. J. Phillips, T. C. Sangster, M. S. Singh, M. A. Stoyer, M. Tabak, G. L. Tietbohl, M. Tsukamoto, K. Wharton, and S. C. Wilks, “Hot electron production and heating by hot electrons in fast ignitor research”, *Physics of Plasmas*, 5, 1966–1972 (1998).
- 30 A. R. Bell, J. R. Davies, S. Guerin, and H. Ruhl, “Fast-electron transport in high-intensity short-pulse laser-solid experiments”, *Plasma Physics and Controlled Fusion*, 39, 653–659 (1997).

-
- 31 D. Batani, J. R. Davies, A. Bernardinello, F. Pisani, M. Koenig, T. A. Hall, S. Ellwi, P. Norreys, S. Rose, A. Djaoui, and D. Neely, “Explanations for the observed increase in fast electron penetration in laser shock compressed materials”, *Physical Review E*, 61, 5725–5733 (2000).
- 32 F. Pisani, A. Bernardinello, D. Batani, A. Antonicci, E. Martinolli, M. Koenig, L. Gremillet, F. Amiranoff, S. Baton, J. Davies, T. Hall, D. Scott, P. Norreys, A. Djaoui, C. Rousseaux, P. Fewes, H. Bandulet, and H. Pepin. “Experimental evidence of electric inhibition in fast electron penetration and of electric-field-limited fast electron transport in dense matter”, *Physical Review E*, 62, R5927–R5930 (2000).
- 33 R. Tommasini, E. E. Fill, R. Bruch, and G. Pretzler, “Generation of monoenergetic ultrashort electron pulses from a fs laser plasma”, *Applied Physics B*, 79, 923–926 (2004).
- 34 E. E. Fill, S. Trushin, R. Bruch, and R. Tommasini, “Diffraction of laser-plasma-generated electron pulses”, *Applied Physics B*, 81:155–157 (2005).
- 35 M. Galimberti, A. Giulietti, D. Giulietti, and L. A. Gizzi, “Sheeba: a spatial high-energy electron beam analyzer”, *Review of Scientific Instruments*, 76, 053303 (2005).
- 36 S. Agostinelli, J. Allison, K. Amako, J. Apostolakis, H. Araujo, P. Arce, and et al. “Geant4 -a simulation toolkit” *Nuclear Instruments and Methods in Physics Research A*, 506, 250–303 (2003).
- 37 L.A.Gizzi , D.Giulietti, A.Giulietti, T.Afshar-Rad, V.Biancalana, P.Chessa, E.Schifano, S.M.Viana, O.Willi, “Characterisation of Laser Plasmas for Interaction Studies”, *Phys. Rev. E*, 49, 5628 (1994), *erratum* 50, 4266 (1994).
- 38 L. Labate, M. Galimberti, A. Giulietti, D. Giulietti, L.A. Gizzi, P. Köster, S. Laville, P. Tomassini, “Ray-tracing simulations of a bent crystal X-ray optics for imaging using laser-plasma X-ray sources”, *Laser Part. Beams* 22, 253 (2004).
- 39 S. A. Pikuz, T. A. Shelkovenko, V. M. Romanova, D. A. Hammer, A. Y. Faenov, V. A. Dyakin, and T. A. Pikuz, “Monochromatic x-ray probing of an ultradense plasma”, *JETP Lett.* 61, 638–644 (1995).
- 40 L. Labate, M. Galimberti, A. Giulietti, D. Giulietti, L.A. Gizzi, P. Tomassini, and G. Di Cocco, “A laser-plasma source for ccd calibration in the soft x-ray range”, *Nuclear Instruments and Methods in Physics Research A*, 495, 148–153, (2002).
- 41 S.C. Wilks, W.L. Kruer, M.Tabak, A.B.Langdon, “Absorption of Ultraintense Laser Pulses”, *Phys. Rev. Lett.* 69, 1383 (1992).
- 42 T. Feurer, A. Morak, I. Uschmann, C. Ziener, H. Schwoerer, C Reich, P. Gibbon, E. Forster, R. Sauerbrey, K. Ortner, C.R. Becker, “Femtosecond silicon K alpha pulses from laser-produced plasmas”, *Phys. Rev. E*, 65, 016412 (2001).
- 43 Ch. Reich, P. Gibbon, I. Uschmann, and E. Foerster “Yield optimization and time structure of femtosecond laser plasma $K\alpha$ sources”, *Physical Review Letters*, 84, 4846–4849 (2000).
- 44 J. Zhang, J. Zhang, Z. M. Sheng, Y. T. Li, Y. Qiu, Z Jin, and H. Teng, “Emission direction of fast electrons in laser-solid interactions at intensities from the nonrelativistic to the relativistic”, *Physical Review E*, 69,046408 (2004).
- 45 G. J. Pert, “Algorithms for the self-consistent generation of magnetic fields in plasmas”, *Journal of Computational Physics*, 43:111–163, 1981.
- 46 L. M. Chen, J. Zhang, Q. L. Dong, H. Teng, T. J. Liang, L. Z. Zhao, and Z. Y. Wei, “Hot electron generation via vacuum heating process in femtosecond laser-solid interactions”, *Physics of Plasmas*, 8:2925, 2001.
- 47 Q. L. Dong, J. Zhang, and H. Teng “Absorption of femtosecond laser pulses in interaction with solid targets” *Physical Review E*, 64, 026411, (2001)
- 48 L.A.Gizzi, D.Batani, V.Biancalana, A.Giulietti, D.Giulietti, “X-Ray emission from Thin Foil Laser produced Plasmas”, *Laser and Particle Beams*, 10, 65 (1992).
- 49 A. Tarasevitch, C. Dietrich, C. Blome, K. Sokolowski-Tinten, and D. von der Linde, “3/2 harmonic generation by femtosecond laser pulses in steep-gradient plasmas” *Physical Review A*, 68, 026410, (2003); L. Veisz, W. Theobald, T. Feurer, H. Schwoerer, I. Uschmann, O. Renner, and R. Sauerbrey, “Three-halves harmonic emission from femtosecond laser produced plasmas with steep density gradients”. *Physics of Plasmas*, 11(6), 3311–3323 (2004).
- 50 A.Giulietti, D.Giulietti, D.Batani, V.Biancalana, L.Gizzi, L.Nocera and E.Schifano, “Spectroscopic Evidence for Sum Frequency of Forward and Backscattered Light in Laser Plasmas”, *Phys. Rev. Lett.* 63, 524 (1989).